Acoustic scattering in case of random obstacles

H. Harbrecht, N. Ilić and M. D. Multerer

Departement Mathematik und Informatik
Fachbereich Mathematik
Universität Basel
CH-4051 Basel

Preprint No. 2018-12
June 2018

www.math.unibas.ch

ACOUSTIC SCATTERING IN CASE OF RANDOM OBSTACLES

HELMUT HARBRECHT, NICOLA ILIĆ, AND MICHAEL D. MULTERER

Abstract. In this article, we deal with the numerical solution of acoustic scattering problems in case of random obstacles. We compute the second order statistics, i.e. the expectation and the variance, of the solution's Cauchy data on an artificial, deterministic interface by means of boundary integral equations. As a consequence, we are able to rapidly evaluate statistics of the scattered wave everywhere in the exterior domain, including the expectation and the variance of the far-field. By using a low-rank approximation of the Cauchy data's two-point correlation function, the cost of the computation of the scattered wave's variance is drastically reduced. Numerical results are given to demonstrate the feasibility of the proposed approach.

1. Introduction

The propagation of an acoustic wave in a homogeneous, isotropic, and inviscid fluid is approximately described by a velocity potential $U(\mathbf{x},t)$ satisfying the wave equation

$$U_{tt} = c^2 \Delta U.$$

Here, c denotes the speed of sound, $\mathbf{v} = \nabla U$ is the velocity field, and $p = -U_t$ is the pressure, see [4] for instance. If U is time harmonic, that is

$$U(\mathbf{x},t) = \mathrm{Re}\left(u(\mathbf{x})e^{-i\omega t}\right), \quad \omega > 0,$$

in complex notation, then the complex-valued space-dependent function u satisfies the Helmholtz equation

$$\Delta u + \kappa^2 u = 0 \quad \text{in } \mathbb{R}^2 \setminus \overline{D}.$$

Here, $D \subset \mathbb{R}^2$ describes an obstacle and $\kappa = \omega/c$ is the wavenumber. We assume that D is bounded and simply connected, having a smooth boundary $\Gamma = \partial D$. For *sound-soft* obstacles the pressure p vanishes on Γ, which leads to the Dirichlet boundary condition

$$u = 0 \quad \text{on } \Gamma.$$

We shall consider the situation that the total wave

$$u = u_i + u_s$$

is comprised of a known incident plane wave $u_i(\mathbf{x}) = e^{i\kappa\langle \mathbf{d},\mathbf{x}\rangle}$ with direction $\mathbf{d}$, where $\|\mathbf{d}\|_2 = 1$, and a scattered wave u_s. Then, if we impose the *Sommerfeld radiation condition*

$$\sqrt{r}\left(\frac{\partial u_s}{\partial r} - i\kappa u_s\right) \to 0 \text{ as } r := \|\mathbf{x}\|_2 \to \infty, \tag{1.1}$$

for the scattered wave, we obtain a unique solution to the acoustic scattering problem

$$\begin{aligned} \Delta u + \kappa u &= 0 \quad \text{in } \mathbb{R}^2 \setminus \overline{D}, \\ u &= 0 \quad \text{on } \Gamma, \\ \sqrt{r}\left(\frac{\partial u_s}{\partial r} - i\kappa u_s\right) &\to 0 \quad \text{as } r = \|\mathbf{x}\|_2 \to \infty, \end{aligned} \tag{1.2}$$

see [4]. Note that the Sommerfeld radiation condition implies the asymptotic behavior

$$u_s(\mathbf{x}) = \frac{e^{i\kappa r}}{r}\left\{u_\infty\left(\frac{\mathbf{x}}{r}\right) + \mathcal{O}\left(\frac{1}{r}\right)\right\}, \quad r \to \infty. \tag{1.3}$$

A function which satisfies (1.2) is called a radiating solution to the Helmholtz equation. The function

$$u_\infty \colon \mathbb{S}^1 := \{\hat{\mathbf{x}} \in \mathbb{R}^2 : \|\hat{\mathbf{x}}\|_2 = 1\} \to \mathbb{C}$$

is called the *far-field pattern*, which is always analytic in accordance with [4].

In this article, we consider the situation that the scatterer D is randomly shaped, i.e. $D = D(\mathbf{y})$ for a random parameter $\mathbf{y} \in \Gamma \subset \mathbb{R}^{\mathbb{N}}$. Hence, the scattered wave itself becomes a random field $u_s(\mathbf{y})$. We will model a class of random domains and compute the associated expected scattered wave $\mathbb{E}[u_s]$ and also the expected far-field $\mathbb{E}[u_\infty]$. Instead of employing the domain mapping method, which maps the deformed scatterer onto a fixed reference domain, as in e.g. [10], we will compute all samples for the deformed scatterer by means of the boundary element method. This approach is much cheaper since we do not require a very fine triangulation for D in order to ensure that the domain deformation field is properly resolved. Consequently, we are also able to deal with large variations without the need of a very fine discretization.

Furthermore, we demonstrate how to compute the scattered wave's second order statistics in a deterministic fashion from its Cauchy data's second order statistics on an artificial, deterministic interface Σ, which almost surely contains the domain $D(\mathbf{y})$. The application of a low-rank approximation for the correlation function greatly decreases the cost to compute the expected scattered field and its variance. The advantages of the proposed approach are thus as follows:

(i) The use of boundary integral equations facilitates a straightforward treatment of the unbounded exterior domain. Especially, it avoids expensive mesh generation procedures in case of strongly varying scatterers.
(ii) Since the artificial interface is bounded and has one dimension less compared to exterior domain, the impact of the high dimensionality of the random scattering problem is drastically reduced.

We like to emphasize that the present approach will also be suitable to treat sound-hard scatterers, where the Dirichlet boundary condition in (1.2) becomes a Neumann condition. Also scatterers with a different diffractive index κ can be considered. The latter leads to a transmission condition at the scatterer's surface instead of a boundary condition. The presented ideas remain valid in this situation except for modifying the boundary integral equations accordingly. Moreover, all concepts can be transferred to the three-dimensional situation, but technicalities will increase.

The rest of the article is organized as follows. In Section 2, we discuss the formulation of the scattering problem under consideration for a deterministic scatterer by means of boundary integral equations and provide a representation of the total wave and the far field pattern. Then, in Section 3, we introduce the random scatterer and provide the expressions to compute the scattered wave's expectation and variance, including the far-field pattern. Section 4 is dedicated to numerical results which quantify and qualify our approach. The boundary integral equations are discretized by the Nyström method which converges exponentially in case of analytic boundaries. Especially, we discuss the efficient computation of the scattered wave's variance by using a low-rank approximation. Finally, in Section 5, we state concluding remarks.

2. Boundary integral equations

2.1. **Computing the scattered wave.** We shall recall the solution of the boundary value problem (1.2) by means of boundary integral equations. To that end, for sake of simplicity in representation, we assume here that the domain D is fixed with a smooth boundary $\Gamma = \partial D$.

We introduce the acoustic single layer operator

$$\mathcal{V}\colon H^{-1/2}(\Gamma) \to H^{1/2}(\Gamma), \quad \mathcal{V}\rho := \int_\Gamma \Phi(\cdot, \mathbf{z})\rho(\mathbf{z})\,\mathrm{d}\sigma_{\mathbf{z}}$$

and the acoustic double layer operator

$$\mathcal{K}\colon L^2(\Gamma) \to L^2(\Gamma), \quad \mathcal{K}\rho := \int_\Gamma \frac{\partial\Phi(\cdot, \mathbf{z})}{\partial \mathbf{n}_{\mathbf{z}}}\rho(\mathbf{z})\,\mathrm{d}\sigma_{\mathbf{z}}.$$

Here, $\Phi(\cdot,\cdot)$ denotes the fundamental solution of the Helmholtz equation. It reads in two spatial dimensions as

$$\Phi(\mathbf{x},\mathbf{z}) = \frac{i}{4} H_0^{(1)}(\kappa\|\mathbf{x}-\mathbf{z}\|_2),$$

where $H_0^{(1)}$ denotes the zeroth order Hankel function of the first kind.

Being given the incident wave $u_i(\mathbf{x}) = e^{i\kappa\langle\mathbf{d},\mathbf{x}\rangle}$, the Neumann data of the total wave $u = u_i + u_s$ at the boundary Γ can be determined by the boundary integral equation

$$\left(\frac{1}{2} + \mathcal{K}^\star - i\eta\mathcal{V}\right)\frac{\partial u}{\partial \mathbf{n}} = \frac{\partial u_i}{\partial \mathbf{n}} - i\eta u_i \quad \text{on } \Gamma, \tag{2.1}$$

see [4].

From the Cauchy data of u at Γ, we can determine the scattered wave u_s in any point in the exterior of the scatterer by applying the potential evaluation

$$u_s(\mathbf{x}) = \int_\Gamma \Phi(\mathbf{x},\mathbf{z})\frac{\partial u}{\partial \mathbf{n}}(\mathbf{z})\,\mathrm{d}\sigma_{\mathbf{z}}, \quad \mathbf{x}\in\mathbb{R}^2\setminus\overline{D}. \tag{2.2}$$

By letting $\|\mathbf{x}\|_2$ tend to infinity in (2.2), we derive a closed expression for the far-field of the total field u. Namely, the far-field at a point $\widehat{\mathbf{x}}\in\mathbb{S}^1$ is given in accordance with

$$u_\infty(\hat{\mathbf{x}}) = \int_\Gamma \Phi_\infty(\hat{\mathbf{x}},\mathbf{z})\frac{\partial u}{\partial \mathbf{n}}(\mathbf{z})\,\mathrm{d}\sigma_{\mathbf{z}}. \tag{2.3}$$

Herein, the far-field kernel $\Phi_\infty(\cdot,\cdot)$ reads as

$$\Phi_\infty(\hat{\mathbf{x}},\mathbf{z}) = -\frac{e^{i\pi/4}}{\sqrt{8\kappa\pi}} e^{-i\kappa\langle\hat{\mathbf{x}},\mathbf{z}\rangle}.$$

2.2. **Alternative representation of the scattered wave.** We shall introduce the circle

$$\Sigma := \{\mathbf{x}\in\mathbb{R}^2 : \|\mathbf{x}\|_2 = R\}$$

of radius $R>0$, being sufficiently large to guarantee that Σ encloses the domain D. By differentiating (2.2), it is seen that the gradient of the scattered wave can simply be computed by

$$\nabla u_s(\mathbf{x}) = \int_\Gamma \nabla_{\mathbf{x}}\Phi(\mathbf{x},\mathbf{z})\frac{\partial u}{\partial \mathbf{n}}(\mathbf{z})\,\mathrm{d}\sigma_{\mathbf{z}}, \quad \mathbf{x}\in\Sigma.$$

Thus, we can compute the Cauchy data of the scattered wave at the artificial interface Σ. It especially holds

$$\frac{\partial u_s}{\partial \mathbf{n}}(\mathbf{x}) = \int_\Gamma \frac{\partial\Phi(\mathbf{x},\mathbf{z})}{\partial \mathbf{n}_{\mathbf{x}}}\frac{\partial u}{\partial \mathbf{n}}(\mathbf{z})\,\mathrm{d}\sigma_{\mathbf{z}}, \quad \mathbf{x}\in\Sigma,$$

where $\mathbf{n}_{\mathbf{x}} = \mathbf{x}/\|\mathbf{x}\|_2$ is the outward normal of Σ at the point $\mathbf{x}\in\Sigma$.

For any $\mathbf{x} \in \mathbb{R}^2$ with $\|\mathbf{x}\|_2 > R$, we can now either use the representation formula (2.2) or the representation formula

$$u_s(\mathbf{x}) = \int_\Sigma \left\{ \Phi(\mathbf{x}, \mathbf{z}) \frac{\partial u_s}{\partial \mathbf{n}}(\mathbf{z}) + \frac{\partial \Phi(\mathbf{x}, \mathbf{z})}{\partial \mathbf{n}_\mathbf{z}} u_s(\mathbf{z}) \right\} \mathrm{d}\sigma_\mathbf{z} \tag{2.4}$$

to compute the scattered wave u_s in any point $\mathbf{x} \in \mathbb{R}^2$ with $\|\mathbf{x}\|_2 > R$. In particular, letting $R \to \infty$, we obtain for the far-field the formula

$$u_\infty(\hat{\mathbf{x}}) = \int_\Sigma \left\{ \Phi_\infty(\hat{\mathbf{x}}, \mathbf{z}) \frac{\partial u}{\partial \mathbf{n}}(\mathbf{z}) + \frac{\partial \Phi_\infty(\mathbf{x}, \mathbf{z})}{\partial \mathbf{n}_\mathbf{z}} u(\mathbf{z}) \right\} \mathrm{d}\sigma_\mathbf{z}, \quad \hat{\mathbf{x}} \in \mathbb{S}^1. \tag{2.5}$$

As we will see, the major advantage of (2.4) and (2.5) over (2.2) and (2.3) is that the circle Σ is fixed in contrast to the shape of the random scatterer later on.

We emphasize that an artificial interface being different from a circle can of course be chosen as well.

3. Random obstacles

3.1. **Star-like obstacles.** From now on, without loss of generality, we restrict ourselves to scatterers D which are star-like with respect to the origin $\mathbf{0} \in \mathbb{R}^2$. Then, we can represent the boundary Γ by the parametrization of the form

$$\boldsymbol{\gamma} \colon [0, 2\pi] \to \mathbb{R}^2, \quad \boldsymbol{\gamma}(\phi) = r(\phi)\mathbf{e}_r(\phi), \tag{3.1}$$

where $\mathbf{e}_r(\phi) = [\cos(\phi), \sin(\phi)]^\top$ denotes the radial direction and $r \in C^2_{\mathrm{per}}([0, 2\pi])$ is a radial function such that $r > 0$. In particular, we may assume that the radial function is given by the possibly infinite Fourier series

$$r(\phi) = \frac{a_0}{2} + \sum_{k=1}^{\infty} \big\{ a_{2k-1} \sin(k\phi) + a_{2k} \cos(k\phi) \big\}$$

with certain coefficients $a_k \in \mathbb{R}$. Especially, from

$$\|\cos(k\phi)\|_{W^{n,\infty}([0,2\pi])} \leq c(n)k^n, \quad \|\sin(k\phi)\|_{W^{n,\infty}([0,2\pi])} = c(n)k^n$$

for all $k \in \mathbb{N}$, we conclude $r \in C^n_{\mathrm{per}}([0, 2\pi])$ if and only if

$$\sum_{k=1}^{\infty} k^n \big\{ |a_{2k-1}| + |a_{2k}| \big\} < \infty.$$

3.2. **Random boundaries.** In what follows, let $(\Omega, \mathcal{F}, \mathbb{P})$ denote a complete and separable probability space with σ-algebra $\mathcal{F}$ and probability measure $\mathbb{P}$. Here, complete means that $\mathcal{F}$ contains all $\mathbb{P}$-null sets. Then, for a given complex Banach space X, we introduce the *Lebesgue-Bochner space* $L^p_{\mathbb{P}}(\Omega; X)$, $1 \leq p \leq \infty$, which consists of all equivalence classes of strongly measurable functions $v\colon \Omega \to X$ whose norm

$$\|v\|_{L^p_{\mathbb{P}}(\Omega;X)} := \begin{cases} \left(\int_\Omega \|v(\cdot,\omega)\|_X^p \,\mathrm{d}\mathbb{P}(\omega)\right)^{1/p}, & p < \infty \\ \operatorname*{ess\,sup}_{\omega\in\Omega} \|v(\cdot,\omega)\|_X, & p = \infty \end{cases}$$

is finite. If $p = 2$ and X is a separable Hilbert space, then the Bochner space is isomorphic to the tensor product space $L^2_{\mathbb{P}}(\Omega) \otimes X$. Note that, for notational convenience, we will always write $v(\mathbf{x}, \omega)$ instead of $\big(v(\omega)\big)(\mathbf{x})$ if $v \in L^p_{\mathbb{P}}(\Omega; X)$. For more details on Lebesgue-Bochner spaces, we refer the reader to [9].

For $p \geq 2$ and a given *random field* $v \in L^p(\Omega; X)$, we can introduce the *expectation*

$$\mathbb{E}[v](\mathbf{x}) := \int_\Omega v(\mathbf{x}, \omega) \,\mathrm{d}\mathbb{P}(\omega)$$

and its *variance*

$$\mathbb{V}[v](\mathbf{x}) := \int_\Omega v(\mathbf{x}, \omega)\overline{v(\mathbf{x}, \omega)} \,\mathrm{d}\mathbb{P}(\omega) - \mathbb{E}[v](\mathbf{x})\overline{\mathbb{E}[v](\mathbf{x})}.$$

With straighforward modifications, these definitions remain valid for real valued random fields.

We assume that the random boundary is determined by replacing the radius function in (3.1) by a real valued random field $r \in L^2\big(\Omega; C^n_{\mathrm{per}}([0, 2\pi])\big)$.

To make a given random field r computationally feasible, we assume that we know in addition to its mean also its covariance function

$$\mathbb{C}\mathrm{ov}[r](\phi, \phi') := \int_\Omega \big(r(\phi, \omega) - \mathbb{E}[r](\phi)\big)\big(r(\phi', \omega) - \mathbb{E}[r](\phi')\big) \,\mathrm{d}\mathbb{P}(\omega).$$

Then, we can compute the *Karhunen-Loève expansion*, cf. [17],

$$r(\phi, \omega) = \mathbb{E}[r](\phi) + \sum_{k=1}^\infty \sqrt{\lambda_k} r_k(\phi) X_k(\omega),$$

where $\{(\lambda_k, r_k)\}_k$ are the eigenpairs of the integral operator with kernel $\mathbb{C}\mathrm{ov}[r]$ and $\{X_k\}_k$ are uncorrelated and centered random variables. An efficient way to compute the Karhunen-Loève expansion is given by the *pivoted Cholesky decomposition*, see [7, 8].

We make the usual assumption that the random variables $\{X_k\}_k$ are also independent and uniformly distributed, i.e. $X_k \sim \mathcal{U}(-1,1)$. Thus, we can replace the random variable X_k by their image $y_k \in [-1,1]$ and obtain the parametrized random field

$$r(\phi, \mathbf{y}) = \mathbb{E}[r](\phi) + \sum_{k=1}^{\infty} \sqrt{\lambda_k} r_k(\phi) y_k.$$

The corresponding image measure μ is given by the product of the push forward measure $\nu = {}^{\mathrm{d}y}/_2$ according to $\mu := \otimes_{k=1}^{\infty} \nu$.

To be consistent with the representation of the radius function in Paragraph 3.1, we shall assume in what follows that the random radius function under consideration ist given by

$$r(\phi, \mathbf{y}) = r_0(\phi) + \sum_{k=1}^{\infty} \big\{ a_{2k-1} y_{2k-1} \sin(k\phi) + a_{2k} y_{2k} \cos(k\phi) \big\}. \tag{3.2}$$

Herein, $\mathbf{y} \in [-1,1]^{\mathbb{N}}$ is the image of the random variables, the numbers $\{a_k^2\}_k$ to the eigen values of the covariance operator and the functions $\{\sin(k\phi), \cos k\phi\}_k$ to its eigen functions.

By construction, the random fluctuations of the radius (3.2) are centered, i.e., their mean vanishes, and we conclude

$$\mathbb{E}[r](\phi) = \int_{[-1,1]^{\mathbb{N}}} r(\phi, \mathbf{y}) \, \mathrm{d}\mu = r_0(\phi).$$

In order to guarantee that each realization $\mathbf{y} \in [-1,1]^{\mathbb{N}}$ results in a domain $D(\mathbf{y})$, we shall further assume

$$0 < \underline{r} \leq r(\phi, \mathbf{y}) \leq \overline{r} < \infty \quad \text{for all } \phi \in [0, 2\pi] \text{ and } \mathbf{y} \in [-1,1]^{\mathbb{N}}. \tag{3.3}$$

Moreover, it is assumed that $r_0 \in C^2_{\mathrm{per}}([0,2\pi])$ as well as that the sequence $(a_k)_k$ decays sufficiently fast to ensure $r(\cdot, \mathbf{y}) \in C^2_{\mathrm{per}}([0,2\pi])$ for all $\mathbf{y} \in [-1,1]^{\mathbb{N}}$.

The *random boundary* $\Gamma = \Gamma(\mathbf{y})$ is hence given by

$$\Gamma(\mathbf{y}) = \big\{ r(\phi, \mathbf{y}) \mathbf{e}_r(\phi) \in \mathbb{R}^2 : \phi \in [0, 2\pi] \big\}$$

with the associated *random scatterer* $D = D(\mathbf{y})$. The *expectation* of the random scatterer is obviously given by the domain which is bounded by $\Gamma(\mathbf{0})$.

Having the incident wave u_i at hand, the boundary value problem for the total field $u(\mathbf{y}) = u_s(\mathbf{y}) + u_i$ for any $\mathbf{y} \in [-1,1]^{\mathbb{N}}$ reads

$$\begin{aligned} \Delta u(\mathbf{y}) + \kappa u(\mathbf{y}) &= 0 \quad \text{in } \mathbb{R}^2 \setminus \overline{D(\mathbf{y})}, \\ u(\mathbf{y}) &= 0 \quad \text{on } \Gamma(\mathbf{y}), \\ \sqrt{r}\left(\frac{\partial u_s}{\partial r} - i\kappa u_s\right) &\to 0 \quad \text{as } r = \|\mathbf{x}\|_2 \to \infty. \end{aligned} \tag{3.4}$$

By the construction of $\Gamma(\mathbf{y})$, the random scattering problem (3.4) exhibits a unique solution for each realization $\mathbf{y} \in [-1,1]^{\mathbb{N}}$ of the random parameter. Moreover, it has been shown in [10] the case of the Helmholtz transmission problem that the total wave $u(\mathbf{y})$ exhibits an anlytic extension into a certain region of the complex plane with respect to the parameter $\mathbf{y} \in [-1,1]^{\mathbb{N}}$. This particularly allows for the use of higher order quadrature methods, like the quasi-Monte Carlo methods, see e.g. [2], or sparse quadrature methods, see e.g. [6, 10] in order to compute quantities of interest, such as expectation and variance.

3.3. **Expected scattered wave.** We can compute the scattered wave's expectation for a given point $\mathbf{x} \in \mathbb{R}^2$ via the potential evaluation (2.2), which leads to

$$\mathbb{E}[u_s](\mathbf{x}) = \mathbb{E}\left[\int_{\Gamma(\mathbf{y})} \Phi(\mathbf{x},\mathbf{z}) \frac{\partial u_s}{\partial \mathbf{n}}(\mathbf{z},\cdot)\,\mathrm{d}\sigma_{\mathbf{z}}\right]. \tag{3.5}$$

Of course, (3.5) makes only sense if $\|\mathbf{x}\| > \overline{r}$ since otherwise there might be instances $\mathbf{y} \in [-1,1]^{\mathbb{N}}$ such that $\mathbf{x} \in D(\mathbf{y})$, i.e., the point $\mathbf{x}$ does not lie outside the scatterer almost surely, compare (3.3). Nonetheless, if we want to compute the expectation in many points, it is much more efficient to exploit the artificial but fixed boundary Σ in order to consider expression (2.4). For any $\mathbf{x} \in \mathbb{R}^2$ with $\|\mathbf{x}\| > R$, it holds

$$\mathbb{E}[u_s](\mathbf{x}) = \int_{\Sigma} \left\{ \Phi(\mathbf{x},\mathbf{z}) \mathbb{E}\left[\frac{\partial u_s}{\partial \mathbf{n}}\right](\mathbf{z}) + \frac{\partial \Phi(\mathbf{x},\mathbf{z})}{\partial \mathbf{n}_{\mathbf{z}}} \mathbb{E}[u_s](\mathbf{z}) \right\} \mathrm{d}\sigma_{\mathbf{z}}. \tag{3.6}$$

Therefore, the scattered wave's expectation is completely encoded in the Cauchy data on the artificial boundary Σ. This means that we only need to compute the expected Cauchy data

$$\mathbb{E}[u_s] = \int_{[-1,1]^{\mathbb{N}}} \left\{ \int_{\Gamma(\mathbf{y})} \Phi(\mathbf{x},\mathbf{z}) \frac{\partial u}{\partial \mathbf{n}}(\mathbf{z},\mathbf{y})\,\mathrm{d}\sigma_{\mathbf{z}} \right\} \mathrm{d}\mu \tag{3.7}$$

and

$$\mathbb{E}\left[\frac{\partial u_s}{\partial \mathbf{n}}\right] = \int_{[-1,1]^{\mathbb{N}}} \left\{ \int_{\Gamma(\mathbf{y})} \frac{\Phi(\mathbf{x},\mathbf{z})}{\partial \mathbf{n}_{\mathbf{z}}} u(\mathbf{z},\mathbf{y})\,\mathrm{d}\sigma_{\mathbf{z}} \right\} \mathrm{d}\mu \tag{3.8}$$

of the scattered wave on the artificial boundary Σ, which is of lower spatial dimension than the exterior domain.

In complete analogy to (3.6), the expected far-field pattern is likewise computed by using (2.5):

$$\mathbb{E}[u_\infty](\hat{\mathbf{x}}) = \int_\Sigma \left\{ \Phi_\infty(\hat{\mathbf{x}}, \mathbf{z}) \mathbb{E}\left[\frac{\partial u_s}{\partial \mathbf{n}}(\mathbf{z})\right] + \frac{\partial \Phi_\infty(\mathbf{x}, \mathbf{z})}{\partial \mathbf{n}_\mathbf{z}} \mathbb{E}[u_s](\mathbf{z}) \right\} \mathrm{d}\sigma_\mathbf{z}.$$

3.4. **Computing the solution's variance.** The variance $\mathbb{V}[u_s]$ of the scattered wave u_s at a point $\mathbf{x}$ with $\|\mathbf{x}\| \geq R$ depends nonlinearly on the Cauchy data of u_s at the artificial interface Σ. Nonetheless, we can use the fact that the variance is the trace of the covariance function:

$$\mathbb{V}[u_s](\mathbf{x}) = \mathbb{C}\mathrm{ov}[u_s](\mathbf{x}, \mathbf{x}')\big|_{\mathbf{x}=\mathbf{x}'} = \mathbb{C}\mathrm{or}[u_s](\mathbf{x}, \mathbf{x}')\big|_{\mathbf{x}=\mathbf{x}'} - |\mathbb{E}[u_s](\mathbf{x})|^2. \tag{3.9}$$

Here, the covariance function is given by

$$\begin{aligned} \mathbb{C}\mathrm{ov}[u_s](\mathbf{x}, \mathbf{x}') &= \mathbb{E}\Big[\big(u_s(\mathbf{x}, \cdot) - \mathbb{E}[u_s](\mathbf{x})\big) \overline{\big(u_s(\mathbf{x}', \cdot) - \mathbb{E}[u_s](\mathbf{x}')\big)} \Big] \\ &= \mathbb{E}\big[u_s(\mathbf{x}, \cdot) \overline{u_s(\mathbf{x}', \cdot)}\big] - \mathbb{E}[u_s](\mathbf{x}) \overline{\mathbb{E}[u_s](\mathbf{x}')}, \end{aligned}$$

and, hence,

$$\mathbb{C}\mathrm{or}[u_s](\mathbf{x}, \mathbf{x}') = \mathbb{E}\big[u_s(\mathbf{x}, \cdot) \overline{u_s(\mathbf{x}', \cdot)}\big].$$

The two-point correlation function is a higher-dimensional object, though. But it depends linearly on the second moments of the Cauchy data of the scattered wave on the artificial interface Σ, which greatly simplifies its computation. Namely, defining for $\mathbf{x}, \mathbf{x}' \in \Sigma$ the quantities

$$\begin{aligned} \mathbb{C}\mathrm{or}[u_s](\mathbf{x}, \mathbf{x}') &= \mathbb{E}\left[\left(\int_{\Gamma(\mathbf{y})} \Phi(\mathbf{x}, \mathbf{z}) \frac{\partial u_s}{\partial \mathbf{n}}(\mathbf{z}, \mathbf{y}) \, \mathrm{d}\sigma_\mathbf{z} \right) \overline{\left(\int_{\Gamma(\mathbf{y})} \Phi(\mathbf{x}', \mathbf{z}) \frac{\partial u_s}{\partial \mathbf{n}}(\mathbf{z}, \mathbf{y}) \, \mathrm{d}\sigma_\mathbf{z} \right)} \right], \\ \mathbb{C}\mathrm{or}\left[\frac{\partial u_s}{\partial \mathbf{n}}\right](\mathbf{x}, \mathbf{x}') &= \mathbb{E}\left[\left(\int_{\Gamma(\mathbf{y})} \frac{\partial \Phi(\mathbf{x}, \mathbf{z})}{\partial \mathbf{n}_\mathbf{z}} u_s(\mathbf{z}, \mathbf{y}) \, \mathrm{d}\sigma_\mathbf{z} \right) \overline{\left(\int_{\Gamma(\mathbf{y})} \frac{\partial \Phi(\mathbf{x}', \mathbf{z})}{\partial \mathbf{n}_\mathbf{z}} u_s(\mathbf{z}, \mathbf{y}) \, \mathrm{d}\sigma_\mathbf{z} \right)} \right], \end{aligned}$$

and

$$\begin{aligned} \mathbb{C}\mathrm{or}\left[u_s, \frac{\partial u_s}{\partial \mathbf{n}}\right](\mathbf{x}, \mathbf{x}') &= \overline{\mathbb{C}\mathrm{or}\left[\frac{\partial u_s}{\partial \mathbf{n}}, u_s\right](\mathbf{x}', \mathbf{x})} \\ &= \mathbb{E}\left[\overline{\left(\int_{\Gamma(\mathbf{y})} \Phi(\mathbf{x}, \mathbf{z}) \frac{\partial u_s}{\partial \mathbf{n}}(\mathbf{z}, \omega) \, \mathrm{d}\sigma_\mathbf{z} \right)} \left(\int_{\Gamma(\mathbf{y})} \frac{\partial \Phi(\mathbf{x}', \mathbf{z})}{\partial \mathbf{n}_\mathbf{z}} u_s(\mathbf{z}, \mathbf{y}) \, \mathrm{d}\sigma_\mathbf{z} \right) \right], \end{aligned}$$

we have for any $\|\mathbf{x}\|_2, \|\mathbf{x}'\|_2 > R$ the deterministic expression

$$\begin{aligned}\mathbb{C}\mathrm{or}[u_s](\mathbf{x},\mathbf{x}') = \int_\Sigma \int_\Sigma \Bigg\{ & \Phi(\mathbf{x},\mathbf{z})\overline{\Phi(\mathbf{x}',\mathbf{z}')}\mathbb{C}\mathrm{or}\left[\frac{\partial u_s}{\partial \mathbf{n}}\right](\mathbf{z},\mathbf{z}') \\ & + \Phi(\mathbf{x},\mathbf{z})\overline{\frac{\partial \Phi(\mathbf{x}',\mathbf{z}')}{\partial \mathbf{n}_{\mathbf{z}'}}}\mathbb{C}\mathrm{or}\left[\frac{\partial u_s}{\partial \mathbf{n}}, u_s\right](\mathbf{z},\mathbf{z}') \\ & + \frac{\partial \Phi(\mathbf{x},\mathbf{z})}{\partial \mathbf{n}_{\mathbf{z}}}\overline{\Phi(\mathbf{x}',\mathbf{z}')}\mathbb{C}\mathrm{or}\left[u_s, \frac{\partial u_s}{\partial \mathbf{n}}\right](\mathbf{z},\mathbf{z}') \\ & + \frac{\partial \Phi(\mathbf{x},\mathbf{z})}{\partial \mathbf{n}_{\mathbf{z}}}\overline{\frac{\partial \Phi(\mathbf{x}',\mathbf{z}')}{\partial \mathbf{n}_{\mathbf{z}'}}}\mathbb{C}\mathrm{or}[u_s](\mathbf{z},\mathbf{z}') \Bigg\} \, \mathrm{d}\sigma_{\mathbf{z}'} \, \mathrm{d}\sigma_{\mathbf{z}}.\end{aligned} \tag{3.10}$$

4. Numerical results

4.1. **Random scatterer.** For our numerical experiments, we shall consider a kite-shaped scatterer as nominal obstacle, described by the parametrization

$$\boldsymbol{\gamma}\colon [0,2\pi] \to \Gamma \subset \mathbb{R}^2, \quad \phi \mapsto \boldsymbol{\gamma}(\phi) := \begin{bmatrix} 5\cos(\phi) - 3.25\cos(2\phi) \\ 7.5\sin(\phi) \end{bmatrix}. \tag{4.1}$$

The random boundary is then defined in accordance with

$$\boldsymbol{\gamma}(\phi,\mathbf{y}) = \overline{\boldsymbol{\gamma}}(\phi) + r(\phi,\mathbf{y}) \begin{bmatrix} \cos(\phi) \\ \sin(\phi) \end{bmatrix}, \tag{4.2}$$

where $\overline{\boldsymbol{\gamma}}(\phi)$ denotes the kite-shaped boundary (4.1) and $r(\phi,\mathbf{y})$ is given by the Fourier series

$$r(\phi,\mathbf{y}) = \sum_{k=1}^{\infty} \frac{1}{k^3} \big\{ \sin(k\phi) y_{2k-1} + \cos(k\phi) y_{2k} \big\}. \tag{4.3}$$

For numerical simulation, we truncate this series after 1000 terms.

Notice that the decay of the coefficients of the random fluctuations (4.3) are at the limit case. It would hold $r(\cdot,\mathbf{y}) \in C^2_{\mathrm{per}}([0,2\pi])$ if the decay of the series $(a_k)_k$ was just a little bit higher. A visualization of 1000 samples of this boundary is found in Figure 1.

4.2. **Statistics at the artificial interface.** For the numerical solution of the boundary integral equation (2.1), we apply the Nyström method to discretize the acoustic single and double layer operators. Given the parametrization (4.2) for a specific instance $\mathbf{y} \in [-1,1]^{1000}$, the method applies the trapezoidal rule in the $n = 1000$ equidistantly distributed points $\varphi_i = {}^{2\pi i}/_{n}$, $i = 1,\dots,n$, and is along the lines of [16]. An appropriate desingularization technique based on trigonometric Lagrange polynomials is employed to deal with the singularities of the acoustic single and double

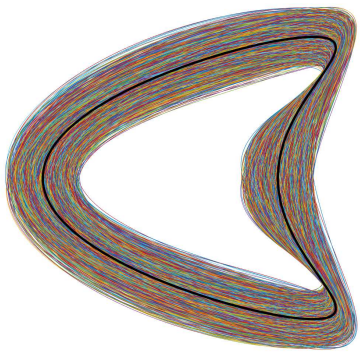

FIGURE 1. The kite-shaped boundary (thick black line) and 1000 random perturbations (in colour).

layer operators. The method converges exponentially provided that the boundary under consideration is analytical. We refer the reader to [16] for all the details.

We likewise subdivide the artificial interface

$$\Sigma = \{\mathbf{x} \in \mathbb{R}^2 : \|\mathbf{x}\|_2 = R\}$$

in $n = 1000$ equidistantly distributed points

$$\mathbf{z}_j = \left[R\cos(2\pi j/n), R\sin(2\pi j/n)\right]^\top, \quad j = 1, \dots, n.$$

In these points, we compute the expectations $\mathbb{E}[u_s](\mathbf{z}_j)$ and $\mathbb{E}[\partial u_s/\partial \mathbf{n}](\mathbf{z}_j)$ in accordance with (3.7) and (3.8), respectively, by the quasi-Monte Carlo method based on 10 000 Halton points, cf. [18]. Moreover, we compute the related two-point correlation matrix

$$\mathbf{C} = \begin{bmatrix} \mathbf{C}_{1,1} & \mathbf{C}_{1,2} \\ \mathbf{C}_{1,2}^\star & \mathbf{C}_{2,2} \end{bmatrix} \in \mathbb{C}^{2n\times 2n}, \tag{4.4}$$

where

$$\mathbf{C}_{1,1} := \left[\mathbb{C}\mathrm{or}[u_s](\mathbf{z}_j, \mathbf{z}_{j'})\right]_{j,j'=1}^n, \quad \mathbf{C}_{2,2} := \left[\mathbb{C}\mathrm{or}\left[\frac{\partial u_s}{\partial \mathbf{n}}\right](\mathbf{z}_j, \mathbf{z}_{j'})\right]_{j,j'=1}^n$$

and

$$\mathbf{C}_{1,2} := \left[\mathbb{C}\mathrm{or}\left[u_s, \frac{\partial u_s}{\partial \mathbf{n}}\right](\mathbf{z}_j, \mathbf{z}_{j'})\right]_{j,j'=1}^n.$$

4.3. **Low-rank approximation of the two-point correlation.** While the computation of $\mathbb{E}[u_s](\mathbf{x})$ at a point $\mathbf{x}$ with $\|\mathbf{x}\|_2 > R$ by (3.6) is straightforward, the

computation of the variance $\mathbb{V}[u_s](\mathbf{x})$ in accordance with (3.9) amounts to the computation of $\mathbb{C}\mathrm{or}[u_s](\mathbf{x},\mathbf{x})$. This requires the approximation of the double integral over Σ. We apply again the trapezoidal rule, having thus to evaluate

$$\begin{aligned}\mathbb{C}\mathrm{or}[u_s](\mathbf{x},\mathbf{x}) \approx \frac{1}{(2R\pi n)^2}\sum_{j,j'=1}^{n}\Bigg\{&\Phi(\mathbf{x},\mathbf{z}_j)\overline{\Phi(\mathbf{x},\mathbf{z}_{j'})}\mathbb{C}\mathrm{or}[u_s](\mathbf{z}_j,\mathbf{z}_{j'})\\ &+\Phi(\mathbf{x},\mathbf{z}_j)\overline{\frac{\partial\Phi(\mathbf{x},\mathbf{z}_{j'})}{\partial\mathbf{n}_{\mathbf{z}_{j'}}}}\mathbb{C}\mathrm{or}\left[u_s,\frac{\partial u_s}{\partial\mathbf{n}}\right](\mathbf{z}_j,\mathbf{z}_{j'})\\ &+\overline{\Phi(\mathbf{x},\mathbf{z}_j)}\frac{\partial\Phi(\mathbf{x},\mathbf{z}_{j'})}{\partial\mathbf{n}_{\mathbf{z}_{j'}}}\overline{\mathbb{C}\mathrm{or}\left[u_s,\frac{\partial u_s}{\partial\mathbf{n}}\right](\mathbf{z}_{j'},\mathbf{z}_j)}\\ &+\frac{\partial\Phi(\mathbf{x},\mathbf{z}_j)}{\partial\mathbf{n}_{\mathbf{z}_j}}\overline{\frac{\partial\Phi(\mathbf{x},\mathbf{z}_{j'})}{\partial\mathbf{n}_{\mathbf{z}_{j'}}}}\mathbb{C}\mathrm{or}\left[\frac{\partial u_s}{\partial\mathbf{n}}\right](\mathbf{z}_j,\mathbf{z}_{j'})\Bigg\}.\end{aligned}$$

The respective evaluations of the two-point correlation functions of the Cauchy data on Σ are stored in the matrix $\mathbf{C}$ from (4.4). We conclude that the cost of this naive evaluation scales quadratically in the number of degrees of freedom used on the artificial interface Σ.

In order to speed-up the computations if the variance $\mathbb{V}[u_s](\mathbf{x})$ has to be computed in many points, we propose to compute first a low-rank approximation of the two-point correlation function of the Cauchy data at Σ. In accordance with [7], we apply the pivoted Cholesky decomposition to get a low-rank approximation

$$\mathbf{C} \approx \mathbf{L}\mathbf{L}^\star = \sum_{i=1}^{m}\boldsymbol{\ell}_i\boldsymbol{\ell}_i^\star \tag{4.5}$$

where $\mathbf{L} = [\boldsymbol{\ell}_1,\ldots,\boldsymbol{\ell}_m] \in \mathbb{C}^{2n\times m}$ with $m \leq n$. Note that the truncation error can rigorously be controlled with respect to the trace norm.

Having the low-rank approximation (4.5) at hand, we arrive at

$$\mathbb{C}\mathrm{or}[u_s](\mathbf{x},\mathbf{x}) \approx \frac{1}{(2R\pi n)^2}\sum_{i=1}^{m}\left|\sum_{j=1}^{n}\left[\Phi(\mathbf{x},\mathbf{z}_j)\ell_{i,j}+\frac{\partial\Phi(\mathbf{x},\mathbf{z}_j)}{\partial\mathbf{n}_{\mathbf{z}_j}}\ell_{i,n+j}\right]\right|^2. \tag{4.6}$$

Therefore, the evaluation of $\mathbb{C}\mathrm{or}[u_s](\mathbf{x},\mathbf{x}')$ requires only $\mathcal{O}(nm)$ operations instead of $\mathcal{O}(n^2)$ operations. If $m \ll n$, this reduces the computational cost considerably, especially since m depends only on the desired accuracy and thus only weakly on n.

In order to demonstrate the effect of the low-rank approximation, we consider again the randomly perturbed kite-shaped scatterer, given by (4.2) and (4.3). The radius of the artificial interface is varying in accordance with $R = 11, 12, \ldots, 15$ and the

rank of the low-rank approximation					
R	$\kappa = 1$	$\kappa = 2$	$\kappa = 4$	$\kappa = 8$	$\kappa = 16$
11	48	56	85	131	193
12	39	51	83	131	194
13	35	49	84	132	195
14	32	49	83	131	195
15	31	49	84	132	194

TABLE 1. Ranks m of the low-rank approximation of the two-point correlation of the Cauchy data on Σ for varying radius R and wavenumber κ.

wavenumber is varying in accordance with $\kappa = 1, 2, 4, 8, 16$. The number of equidistant points on Σ is 1000 and and the number of boundary elements on $\Gamma(\mathbf{y})$ is also 1000. Note that the incident wave was chosen to come from the left, i.e., $\mathbf{d} = [1, 0]^\top$, and the relative truncation error was 10^{-12}.

4.4. **Scattered field computation.** We choose $R = 11$ and compute the expectation and variance of the scattered field on the disc $\{\mathbf{x} \in \mathbb{R}^2 : R \leq \|\mathbf{x}\|_2 \leq 50\}$ in accordance with (3.6) and (3.9) using (4.6), where the incident wave comes again from the left, i.e., $\mathbf{d} = [1, 0]^\top$. The results are found in Figure 2. For comparison, the scattered wave in case of the unperturbed kite-shaped scatterer is found in the first column. In the second column, the expected scattered wave is found. Finally, the variance of the scattered wave is found in the third column. The rows correspond to the wavenumber: the first row corresponds to $\kappa = 1$, the second row corresponds to $\kappa = 2$, the third row corresponds to $\kappa = 4$, and the fourth row corresponds to $\kappa = 8$.

One observes that, compared to the scattered wave of the unperturbed scatterer, the expected scattered wave is smoothed towards the left, i.e., contrary to the direction of the incoming wave. This issues from the different reflections at the perturbed scatterer which interfere. In the shadow region, i.e., towards the right, the expected scattered wave and the scattered wave of the unperturbed scatterer basically coincide. This observation is also underpinned by the variance of the scattered wave, which is maximal on the left of the scatterer and nearly 0 in the shadow region. Notice that described smoothing effect becomes stronger as the wavenumber increases.

4.5. **Far-field pattern.** We shall next consider the far-field pattern of the randomly perturbed kite-shape scatterer for the wavenumbers $\kappa = 1, 2, 4, 8$. The far-field has been evaluated in $n = 1000$ equidistant points on $\mathbb{S}^1$. The results of the computations

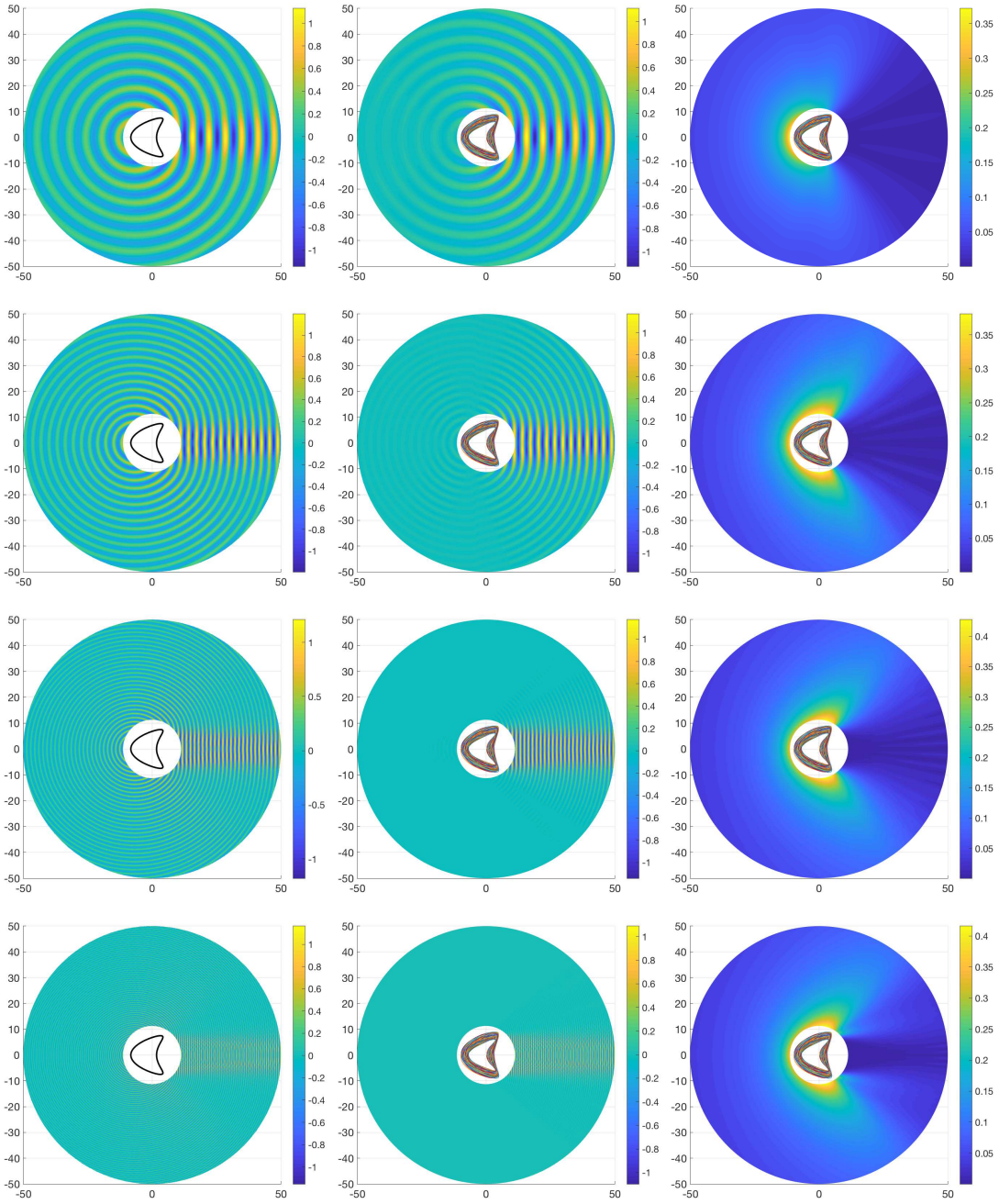

FIGURE 2. The scattered field of a kite-shaped scatterer is found in the left column. The expected scattered field in case of random perturbations is found in the middle column and the associated variance in the right column. The wavenumbers are $\kappa = 1, 2, 4$ and 8, associated with the 1^{st}, 2^{nd}, 3^{rd}, and 4^{th} row.

are found in Figure 3, where we plotted the expected farfield (blue line) and the deviation of the farfield (dash-dotted line). We again observe that the expected farfield pattern does only oscillate in the shadow region, which is in clear contrast to the farfield of the unperturbed kite-shaped scatterer (red line).

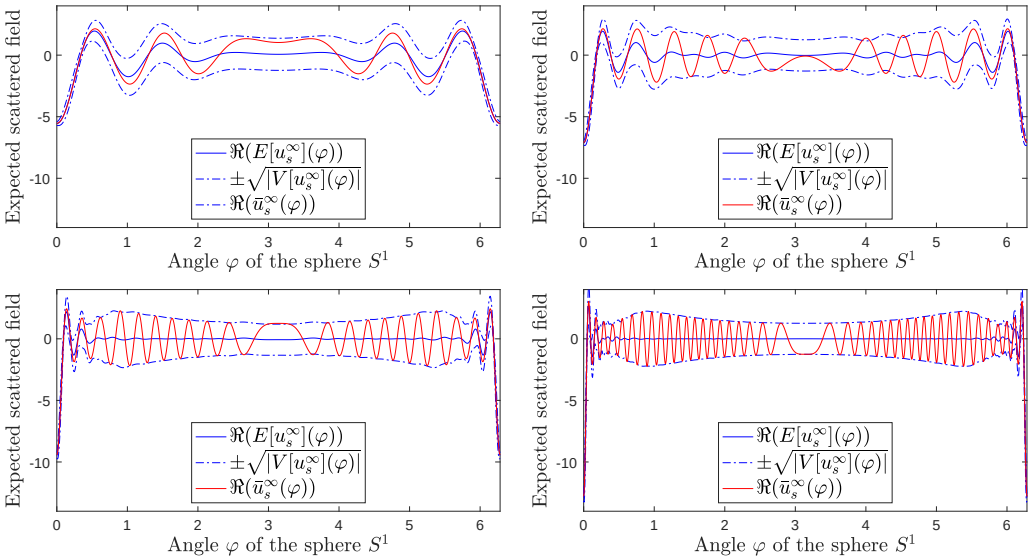

FIGURE 3. The real part of the expected far-field (blue line) with dispersion (blue dash-dotted line) and the far-field of the unperturbed kite shape (red line) in case of $\kappa = 1$ (top left), $\kappa = 2$ (top right), $\kappa = 4$ (bottom left) and $\kappa = 8$ (bottom right).

5. Conclusion

In the present article, acoustic scattering has been considered in case random obstacles. The random scattering problem has been parametrized over the high-dimensional unit cube. We reformulate this random problem, posed in the exterior domain, as a boundary integral equation which yields a dimension reduction. The Nyström method is applied to solve the boundary integral equation for each particular realization. By computing the solution's second order statistics on an artificial, deterministic boundary, the scattered wave's second order statistics can be deterministically determined everywhere, where a low-rank approximation of the covariance matrix greatly improves the efficiency.

The method proposed here can also be formulated for the scattering at sound-hard obstacles. Moreover, it can be extended to other boundary value problems for which a Green's function is available. The observation that the solution's second

order statistics is determined by the second order statistics of the Cauchy data on a deterministic interface holds even for arbitrary second order elliptic boundary value problems.

References

[1] H. Brackhage and P. Werner. Über das Dirichletsche Außenraumproblem für die Helmholtzsche Schwingungsgleichung. *Arch. Math.*, 16:325–329, 1965.

[2] R. Caflisch. Monte Carlo and quasi-Monte Carlo methods. *Acta Numerica*, 7:1–49, 1998.

[3] D. Colton and R. Kress. *Integral equation methods in scattering theory.* John Wiley & Sons, New York, 1983.

[4] D. Colton and R. Kress. *Inverse Acoustic and Electromagnetic Scattering.* Springer, Berlin-Heidelberg-New York, 2nd Edition, 1997.

[5] K. Giebermann. Schnelle Summationsverfahren zur numerischen Lösung von Integralgleichungen für Streuprobleme im $\mathbb{R}^3$. PhD thesis, Universität Karlsruhe (TH), Germany, 1997.

[6] A.-L. Haji-Ali, H. Harbrecht, M. D. Peters, and M. Siebenmorgen. Novel results for the anisotropic sparse grid quadrature. *J. Complexity*, 2018.

[7] H. Harbrecht, M. Peters, and R. Schneider. On the low-rank approximation by the pivoted Cholesky decomposition. *Appl. Numer. Math.*, 62(4):428–440, 2012.

[8] H. Harbrecht, M. Peters, and M. Siebenmorgen. Efficient approximation of random fields for numerical applications. *Numer. Lin. Algebra Appl.*, 22:596–617, 2015.

[9] E. Hille and R. S. Phillips. *Functional analysis and semi-groups.* American Mathematical Society, Providence, RI, 1957.

[10] R. Hiptmair, L. Scarabosio, C. Schillings, and Ch. Schwab. Large deformation shape uncertainty quantification in acoustic scattering. *Adv. Comput. Math.*, 2018, to appear.

[11] A. Kirsch. Surface gradients and continuity properties for some integral operators in classical scattering theory. *Math. Meth. Appl. Sciences*, 11:789–804, 1989.

[12] A. Kirsch. Properties of far field operators in acoustic scattering. *Math. Meth. Appl. Sci.*, 11:773–787, 1989.

[13] A. Kirsch. The domain derivative and two applications in inverse scattering theory. *Inverse Problems*, 9:81–96, 1993.

[14] R. Kress. Minimizing the condition number of boundary integral operators in acoustic and electromagnetic scattering. *Q. J. Mech. Appl. Math.*, 38:323–341, 1985.

[15] R. Kress. A Newton method in inverse obstacle scattering. In Bui et al., editors, *Inverse Problems in Engineering Mechanics*, pages 425–432, Rotterdam, 1994. Balkema.

[16] R. Kress. *Linear Integral Equations.* Applied Mathematical Sciences 82, 3rd edition, Springer, New York, 2014.

[17] M. Loève. *Probability theory. I+II*. Number 45 in Graduate Texts in Mathematics. Springer, New York, 4th edition, 1977.
[18] H. Niederreiter. *Random Number Generation and Quasi-Monte Carlo Methods*. Society for Industrial and Applied Mathematics, Philadelphia, PA, USA, 1992.
[19] W. Tobocman. Inverse acoustic wave scattering in two dimensions from impenetrable targets. *Inverse Problems*, 5:1131–1144, 1989.

Helmut Harbrecht, Departement Mathematik und Informatik, Universität Basel, Spiegelgasse 1, 4051 Basel, Schweiz.

E-mail address: helmut.harbrecht@unibas.ch

Nicola Ilić, Departement Mathematik und Informatik, Universität Basel, Spiegelgasse 1, 4051 Basel, Schweiz.

E-mail address: n.ilic@unibas.ch

Michael D. Multerer, Institute of Computational Science, USI Lugano, Via Giuseppe Buffi 13, 6900 Lugano, Schweiz

E-mail address: michael.multerer@usi.ch

LATEST PREPRINTS

No.	Author: *Title*
2017-06	**P. Zaspel** *Analysis and parallelization strategies for Ruge-Stüben AMG on many-core processor*
2017-07	**H. Harbrecht and M. Schmidlin** *Multilevel Methods for Uncertainty Quantification of Elliptic PDEs with Random Anisotropic Diffusion*
2017-08	**M. Griebel and H. Harbrecht** *Singular value decomposition versus sparse grids: Refined complexity Estimates*
2017-09	**J. Garcke and I. Kalmykov** *Efficient Higher Order Time Discretization Schemes for Hamilton-Jacobi-Bellman Equations Based on Diagonally Implicit Symplectic Runge-Kutta Methods*
2017-10	**M. J. Grote and U. Nahum** *Adaptive Eigenspace Regularization For Inverse Scattering Problems*
2017-11	**J. Dölz, H. Harbrecht, S. Kurz, S. Schöps and F. Wolf** *A Fast Isogeometric BEM for the Three Dimensional Laplace- and Helmholtz Problems*
2017-12	**P. Zaspel** *Algorithmic patterns for $\mathcal{H}$-matrices on many-core processors*
2017-13	**R. Brügger, R. Croce and H. Harbrecht** *Solving a free boundary problem with non-constant coefficients*
2017-14	**M. Dambrine, H. Harbrecht and B. Puig** *Incorporating knowledge on the measurement noise in electrical impedance tomography*
2017-15	**C. Bürli, H. Harbrecht, P. Odermatt, S. Sayasone and N. Chitnis** *Analysis of Interventions against the Liver Fluke, Opisthorchis viverrini*
2017-16	**D. W. Masser** *Abcological anecdotes*
2017-17	**P. Corvaja, D. W. Masser and U. Zannier** *Torsion hypersurfaces on abelian schemes and Betti coordinates*

Preprints are available under *https://math.unibas.ch/research/publications*

LATEST PREPRINTS

No.	Author: *Title*
2017-18	**F. Caubet, M. Dambrine and H. Harbrecht** *A Newton method for the data completion problem and application to obstacle detection in Electrical Impedance Tomography*
2018-01	**H. Harbrecht and P. Zaspel** *On the algebraic construction of sparse multilevel approximations of elliptic tensor product problems*
2018-02	**F. Ghiraldin and X. Lamy** *Optimal Besov differentiability for entropy solutions of the eikonal equation*
2018-03	**H. Harbrecht and M. Schmidlin** *Multilevel quadrature for elliptic problems on random domains by the coupling of FEM and BEM*
2018-04	**M. Bugeanu and H. Harbrecht** *Parametric representation of molecular surfaces*
2018-05	**A. Abdulle, M. J. Grote and O. Jecker** *Finite element heterogeneous multiscale method for Elastic Waves in Heterogeneous Media*
2018-06	**M. J. Grote and J. H. Tang** *On controllability methods for the Helmholtz equation*
2018-07	**H. Harbrecht and M. Moor** *Wavelet boundary element methods — Adaptivity and goal-oriented error estimation*
2018-08	**P. Balazs and H. Harbrecht** *Frames for the solution of operator equations in Hilbert spaces with fixed dual pairing*
2018-09	**R. Brügger, R. Croce and H. Harbrecht** *Solving a Bernoulli type free boundary problem with random diffusion*
2018-10	**J. Dölz, H. Harbrecht and M. D. Multerer** *On the best approximation of the hierarchical matrix product*
2018-11	**H. Harbrecht and P. Zaspel** *A scalable $\mathcal{H}$-matrix approach for the solution of boundary integral equations on multi-GPU clusters*
2018-12	**H. Harbrecht, N. Ilić and M. D. Multerer** *Acoustic scattering in case of random obstacles*

Preprints are available under *https://math.unibas.ch/research/publications*